Interacting quintessence cosmology from Noether symmetries: comparing theoretical predictions with observational data

Ester Piedipalumbo[a,b,*], Stefano Vignolo[c], Pasquale Feola[c], Salvatore Capozziello[a,b,d]

[a]*Dipartimento di Fisica "E. Pancini", Università degli Studi di Napoli "Federico II", Compl. Univ. Monte S. Angelo, Edificio 6, Via Cinthia, I-80126 Napoli, Italy*
[b]*Istituto Nazionale di Fisica Nazionale, Sez. di Napoli, Compl. Univ. Monte S. Angelo, Edificio 6, via Cinthia, I-80126, Napoli, Italy*
[c]*DIME, Università di Genova, Via all' Opera Pia 15, I-16145, Genova, Italy*
[d]*Scuola Superiore Meridionale, Largo S. Marcellino 10, I-80138, Napoli, Italy.*

Abstract

In the framework of scalar-tensor gravity, we consider non–flat interacting quintessence cosmology where a scalar field is interacting with dark matter. Such a scalar field can be a standard or a *phantom* one. We use the Noether Symmetry Approach to obtain general exact solutions for cosmological equations and to select scalar-field self-interaction potentials. It turns out that the found solutions can reproduce the accelerated expansion of the Universe, and are compatible with observational dataset, as the SNeIa Pantheon data, gamma ray bursts Hubble diagram, and direct measurements of the Hubble parameter.

Keywords: Scalar-tensor gravity; Noether symmetries; observational cosmology.

1. Introduction

The detection of the accelerated expansion of the Universe is one of the most challenging discoveries in cosmology over the last decades. To explain this unexpected dynamics, two main proposals have been developed. According to the first approach, the accelerated expansion is driven by some some unknown *dark energy* fluid; the second approach, instead, is connected to non-homogeneous matter distributions or to some modification or extension of General Relativity. According to these perspectives, several cosmological models have been proposed in literature, including a non-zero cosmological constant, standard or *phantom* scalar fields, and extended/alternative theories of gravity [7–15].

Recently interacting dark matter - dark energy models, dubbed as *interacting dark energy* or *coupled-dark energy*, have been proposed in different contexts in view to ad-

---

*Corresponding author
Email addresses:* ester@na.infn.it (Ester Piedipalumbo), stefano.vignolo@unige.it (Stefano Vignolo), capozziello@na.infn.it (Salvatore Capozziello)

dress several cosmological problems, such as the cosmic coincidence problem - i.e. the circumstance that dark energy and dark matter amounts are today of the same order of magnitude, even if they evolve independently- and cosmological tensions ([9, 16–31].) However, these interacting dark energy models are characterized by some phenomenological choices for the interaction form, and there is a certain freedom in choosing specific interaction models. In [31] we investigated, in a flat model, whether this coupling can be selected by the existence of a Noether symmetry. It turned out that this method allows us to select both the analytical form of the interaction and the self-interacting potential of the scalar field: we actually found out that the interaction term can be factorized as $F(a, \phi) = F_1(a)F_2(\phi)$. Moreover, we were able to obtain exact solutions of the Friedman equations, which are quite well compatible with this SNeIa data set. In this paper, we extend the *Noether Symmetry Approach* (see [32] for details) to a cosmological model with non–flat spatial geometry, and to *phantom* scalar fields.

In Section 2, we investigate the existence of Noether symmetries for the point-like Lagrangian describing a single standard or *phantom* scalar field coupled to dark matter. We show that the existence of this symmetry allows a coupled dark energy field and selects the self-interaction potential leading the dark matter-dark energy interaction: we actually obtain more general expressions, and not always factorizable, for the interaction term.

Section 3 is devoted to obtain general exact solutions for the Friedman equations, which naturally supply accelerated expansions.

In Section 4 we finally compare the theoretical solutions with different datasets in order to achieve a reliable cosmic history at different redshifts. In Section 5 we draw conclusions.

2. Interacting scalar-tensor cosmology

The Noether Symmetry Approach [32] provides a geometric selection rule to find out the unknown parameters or functions in the gravitational action, and to solve the cosmological equations [12, 14, 33–40]. Moreover, the existence of a Noether symmetry allows to reduce the dynamical system that, in most cases, results integrable. In the present case, let us consider the following action functional

$$\mathcal{A} = \int \sqrt{-g} \left[-\frac{1}{2}R + \frac{\epsilon}{2}g^{ij}\phi_i\phi_j + V(\phi) + \tilde{\mathcal{L}}(g_{ij}, \phi) \right] d^4x \,, \qquad (1)$$

describing a theory of gravity with a minimally coupled scalar field interacting with the dark matter component. $V(\phi)$ denotes the self–interaction potential of the scalar field ϕ, whereas

$$\tilde{\mathcal{L}}(g_{ij}, \phi) = \mathcal{L}_m(g_{ij}) + \mathcal{L}_m^{int}(g_{ij}, \phi) \,, \qquad (2)$$

is the sum of standard matter Lagrangian function $\mathcal{L}_m(g_{ij})$ with interaction term $\mathcal{L}_m^{int}(g_{ij}, \phi)$. In order to study cosmological models deriving from the action (1), let us take into account a Friedman–Robertson–Walker spacetime, whose line element is expressed as

$$ds^2 = -dt^2 + a(t)^2 \left[\frac{dr^2}{1 - kr^2} + r^2 d\theta^2 + r^2 \sin^2 \theta d\varphi^2 \right] \,, \qquad (3)$$

2

with $k = -1, 0, 1$. Inserting the content of Eq. (3) into Eq. (1), we get the corresponding point–like Lagrangian

$$\mathcal{L}(a, \phi, \dot{a}, \dot{\phi}) = 3a\dot{a}^2 - a^3 \left(\frac{\epsilon \dot{\phi}^2}{2} - V(\phi) \right) - 3ka + Ma^{-3(\gamma-1)} \left(1 + F(a, \phi) \right) , \quad (4)$$

where $\gamma \in [1, 2]$, and the term

$$\mathcal{L}_m(g_{ij}) = Ma^{-3(\gamma-1)} \quad (5)$$

indicates the standard matter Lagrangian function with the constant M related to the present matter density, and

$$\mathcal{L}_m^{int}(g_{ij}, \phi) = Ma^{-3(\gamma-1)} F(a, \phi) , \quad (6)$$

denotes the interaction term. The value of the constant ϵ discriminates between standard and phantom quintessence field: actually, in the former case, it is $\epsilon = 1$ while, in the latter, it is $\epsilon = -1$. The variation with respect to the two dynamical fields a and ϕ gives the Euler-Lagrange equations

$$2\frac{\ddot{a}}{a} + H^2 + \frac{k}{a^2} + \frac{\epsilon \dot{\phi}^2}{2} - V(\phi) + (\gamma - 1) Ma^{-3\gamma} (1 + F) - \frac{1}{3} Ma^{(-3\gamma+1)} \frac{\partial F}{\partial a} = 0 , \quad (7a)$$

$$\epsilon\ddot{\phi} + 3\epsilon H\dot{\phi} + \frac{\partial V}{\partial \phi} + Ma^{-3\gamma} \frac{\partial F}{\partial \phi} = 0 , \quad (7b)$$

where $H = \dfrac{\dot{a}}{a}$ is the Hubble parameter. Moreover, the Jacobi first integral provides the relation

$$3H^2 - \frac{\epsilon \dot{\phi}^2}{2} + \frac{3k}{a^2} - V(\phi) - Ma^{-3\gamma} (1 + F) = 0 , \quad (8)$$

corresponding to the $(0, 0)$ Einstein field equation.

In the case of $\gamma = 1$, we can write Eq.(8) in the form:

$$3H^2 = \rho_m + \rho_k + \rho_\phi^{eff} , \quad (9)$$

where the effective energy density of the ϕ-field is given by

$$\rho_\phi^{eff} = \rho_\phi + Ma^{-3} F(a, \phi) , \quad (10)$$

and ρ_ϕ is the scalar field energy density

$$\rho_\phi = \frac{1}{2}\epsilon\dot{\phi}^2 + V(\phi) . \quad (11)$$

Analogously, it is possible to define an effective pressure of the scalar field as:

$$p_\phi^{eff} = \frac{1}{2}\epsilon\dot{\phi}^2 - V(\phi) + \frac{M}{3a^2} \frac{\partial F(a, \phi)}{\partial a} . \quad (12)$$

3

With these two expressions, it turns out that Eq.(7a) takes the form

$$6\left(\frac{\ddot{a}}{a}\right) = -\left(\rho_{eff} + 3p_{eff}\right),$$ (13)

and it is possible to define an effective equation of state

$$w_\phi^{eff} = \frac{p_\phi}{\rho_\phi} = \frac{\frac{1}{2}\epsilon\dot{\phi}^2 - V(\phi) + \frac{M}{3a^2}\frac{\partial F(a,\phi)}{\partial a}}{\frac{1}{2}\epsilon\dot{\phi}^2 + V(\phi) + Ma^{-3}F(a,\phi)},$$ (14)

which drives the dynamics of the model.

3. Noether symmetries and exact solutions

The system of differential Eqs. (7a),(7b), (8) is non-linear and many choices are possible for the interaction term $F(a,\phi)$ and the self interaction potential $V(\phi)$. In order to solve the system, we search for Noether symmetries for the Lagrangian in Eq. (4), by which it is possible to simplify the study of the dynamics. Furthermore, the existence of these symmetries allows us to fix the forms of $F(a,\phi)$ and $V(\phi)$.

3.1. The case of a standard scalar field

The configuration space of the model is given by the local coordinates. It is $\mathcal{Q} \equiv \{a, \phi\}$. The associated tangent bundle is then given by the fibered coordinates, i.e. $T\mathcal{Q} \equiv \{a, \phi, \dot{a}, \dot{\phi}\}$. The resulting point–like Lagrangian is a function on $T\mathcal{Q}$ having the local expression

$$\mathcal{L}(a, \phi, \dot{a}, \dot{\phi}) = 3a\dot{a}^2 - a^3\left(\frac{\dot{\phi}^2}{2} - V(\phi)\right) - 3ka + Ma^{-3(\gamma-1)}\left(1 + F(a,\phi)\right).$$ (15)

We look for Noether symmetries of the Lagrangian (15) of the form

$$X = \alpha\frac{\partial}{\partial a} + \beta\frac{\partial}{\partial \phi} + \dot{\alpha}\frac{\partial}{\partial \dot{a}} + \dot{\beta}\frac{\partial}{\partial \dot{\phi}}$$ (16)

where $\alpha = \alpha(a,\phi)$, $\beta = \beta(a,\phi)$, $\dot{\alpha} = \dot{a}\frac{\partial\alpha}{\partial a} + \dot{\phi}\frac{\partial\alpha}{\partial \phi}$ and $\dot{\beta} = \dot{a}\frac{\partial\beta}{\partial a} + \dot{\phi}\frac{\partial\beta}{\partial \phi}$. The vector fields (16) are defined on the tangent bundle $T\mathcal{Q}$ and are the canonical lift of corresponding vector fields

$$Y = \alpha\frac{\partial}{\partial a} + \beta\frac{\partial}{\partial \phi}$$ (17)

defined on $\mathcal{Q}$. A Noether symmetry (16) is achieved if the condition

$$X\mathcal{L} = \alpha\frac{\partial\mathcal{L}}{\partial a} + \beta\frac{\partial\mathcal{L}}{\partial \phi} + \dot{\alpha}\frac{\partial\mathcal{L}}{\partial \dot{a}} + \dot{\beta}\frac{\partial\mathcal{L}}{\partial \dot{\phi}} = 0,$$ (18)

holds.

Condition ([18](#)) gives rise to the following system of first–order partial differential equations

$$\alpha + 2a\frac{\partial \alpha}{\partial a} = 0 \tag{19a}$$

$$3\alpha + 2a\frac{\partial \beta}{\partial \phi} = 0 \tag{19b}$$

$$6\frac{\partial \alpha}{\partial \phi} - a^2\frac{\partial \beta}{\partial a} = 0 \tag{19c}$$

$$3\alpha a^2 V(\phi) + \beta a^3\frac{dV}{d\phi}(\phi) - 3(\gamma - 1)Ma^{-3\gamma+2}\alpha\left(1 + F(a, \phi)\right)$$

$$+Ma^{-3(\gamma-1)}\frac{\partial F}{\partial a}\alpha + Ma^{-3(\gamma-1)}\frac{\partial F}{\partial \phi}\beta - 3k\alpha = 0 \tag{19d}$$

Eqs. ([19a](#)), ([19b](#)) and ([19c](#)) can be solved by separating variables. Solutions are

$$\alpha = \frac{Ae^{\frac{1}{2}\sqrt{3/2}\phi} + Be^{-\frac{1}{2}\sqrt{3/2}\phi}}{a^{1/2}} \tag{20a}$$

$$\beta = \frac{-A\sqrt{6}e^{\frac{1}{2}\sqrt{3/2}\phi} + B\sqrt{6}e^{-\frac{1}{2}\sqrt{3/2}\phi}}{a^{3/2}} \tag{20b}$$

where A and B are intergration constants. After, we can split Eqs. ([19d](#)) into two separate equations for $V(\phi)$ and $F(a, \phi)$ respectively:

$$3\alpha a^2 V(\phi) + \beta a^3 V'(\phi) = 0 \tag{21a}$$

and

$$-3(\gamma-1)Ma^{-3\gamma+2}\alpha\left(1 + F(a, \phi)\right) + Ma^{-3(\gamma-1)}\frac{\partial F}{\partial a}\alpha + Ma^{-3(\gamma-1)}\frac{\partial F}{\partial \phi}\beta - 3k\alpha = 0\,. \tag{21b}$$

Therefore, making use of Eqs. ([20](#)), we find the potential

$$V(\phi) = e^{-\sqrt{\frac{3}{2}}\phi}V_0\left(B - Ae^{\sqrt{\frac{3}{2}}\phi}\right)^2\,. \tag{22}$$

Some comments are in order here. These kind of potential is physically relevant because it gives accelerated expansion also for the inflationary paradigm [41]. Furthermore, it is possible to show that exponential forms for the potential result in invertible conformal transformations and can be related to $f(R)$ gravity in the Einstein frame [42]. In the following we set $A = 0$, so that the potential takes the form:

$$V(\phi) = V_0 e^{-\sqrt{3/2}\phi}\,. \tag{23a}$$

The function $F(a, \phi)$ is

$$F(a, \phi) = a^{3(\gamma-1)}G(-\sqrt{6}\ln a + \phi) + \frac{3k}{M}a^{3\gamma-2} - 1\,, \tag{23b}$$

5

where $G(x)$ is an arbitrary function of one real variable. Inserting Eqs. (23a) and (23b) into Eq. (15), Lagrangian (15) assumes the expression

$$\mathcal{L} = a^3 \left(V_0 e^{-\sqrt{\frac{3}{2}}\phi} - \frac{\dot{\phi}^2}{2} \right) + MG \left(\phi - \sqrt{6} \log(a) \right) + 3\dot{a}^2 a \,. \tag{24}$$

It is worth noticing that the above symmetries give rise to an interaction term which actually cancels the contributions due to the spatial curvature and reduces the dynamic effect of the cosmological fluid to that of a dust. The effects of the curvature remain indeed in the evolution of the scalar field, as it can be inferred from the definition of the effective density and pressure of the scalar field (see Eqs. (10) and (12)).

For instance, by choosing $G(x) = Qe^{-\frac{hx}{\sqrt{6}}}$ with Q and h appropriate constants, we have the function

$$F(a, \phi) = Qa^{3(\gamma-1)+h} e^{-\frac{h\phi}{\sqrt{6}}} + \frac{3k}{M} a^{3\gamma-2} - 1 \,. \tag{25}$$

In this case, the Lagrangian (15) assumes the physically relevant expression

$$\mathcal{L} = 3a\dot{a}^2 - a^3 \left(\frac{\dot{\phi}^2}{2} - V_0 e^{-\sqrt{3/2}\phi} \right) + MQa^h e^{-\frac{h\phi}{\sqrt{6}}} \,. \tag{26}$$

It is possible to choose new coordinates, u and v, associated with the Noether symmetry X, in such a way that they satisfy the relations

$$X(u) = 0 \quad \text{and} \quad X(v) = 1 \,. \tag{27}$$

Thus the variable v is cyclic for the transformed Lagrangian (i.e. $\dfrac{\partial \mathcal{L}}{\partial v} = 0$). It turns out that

$$a = (uv)^{1/3} \,, \tag{28a}$$

$$\phi = -\sqrt{2/3}\ln\frac{u}{v} \,. \tag{28b}$$

In terms of the new coordinates, the Lagrangian (26) can be expressed as

$$\mathcal{L} = \frac{4}{3}\dot{u}\dot{v} + V_0 u^2 + MQu^{\frac{2h}{3}} \,, \tag{29}$$

where v is a cyclic coordinate. The associated conserved momentum is given by

$$\frac{\partial \mathcal{L}}{\partial \dot{v}} = \frac{4}{3}\dot{u} = \Sigma \,, \tag{30}$$

where Σ is a constant of motion. By integrating Eq.(30), we get

$$u(t) = \frac{3}{4}\Sigma t + u_0 \,. \tag{31}$$

Using the Jacobi first integral of (29), we obtain the evolution equation for v

$$\dot{v} = \frac{V_0}{\Sigma} \left(\frac{3}{4}\Sigma t + u_0 \right)^2 + \frac{MQ}{\Sigma} \left(\frac{3}{4}\Sigma t + u_0 \right)^{\frac{2h}{3}} \tag{32}$$

which is directly integrated, giving rise to

$$v(t) = \frac{4V_0}{9\Sigma^2}\left(\frac{3}{4}\Sigma t + u_0\right)^3 + \frac{4MQ}{3\Sigma^2\left(\frac{2h}{3}+1\right)}\left(\frac{3}{4}\Sigma t + u_0\right)^{\frac{2h}{3}+1} + C\,. \qquad (33)$$

Therefore, Eqs. (28a) and (28b) provide the analytical form for the scale factor, $a(t)$, and the scalar field, $\phi(t)$ in terms of $u(t)$ and $v(t)$.

Another possible choice in Eq. (23b) is $G(x) = Qx^n$. The point–like Lagrangian (15) becomes

$$\mathcal{L} = 3a\dot{a}^2 - a^3\left(\frac{\dot{\phi}^2}{2} - V_0 e^{-\sqrt{3/2}\phi}\right) + MQ(-\sqrt{6}\ln a + \phi)^n\,. \qquad (34)$$

By performing again the coordinate trasformation (28), the Lagrangian (34) assumes the form

$$\mathcal{L} = \frac{4}{3}\dot{u}\dot{v} + V_0 u^2 + 6^{n/2}MQ\left(-\frac{2}{3}\ln u\right)^n \qquad (35)$$

Again, the variable v is cyclic, the quantity $\dfrac{\partial \mathcal{L}}{\partial \dot{v}} = \dfrac{4}{3}\dot{u}$ is conserved and the solution (31) holds. By inserting solution (31) into the Jacobi first integral, we get the evolution equation for the variable v

$$\dot{v} = \frac{V_0}{\Sigma}\left(\frac{3}{4}\Sigma t + u_0\right)^2 + 6^{n/2}\frac{MQ}{\Sigma}\left(-\frac{2}{3}\ln\left(\frac{3}{4}\Sigma t + u_0\right)\right)^n \qquad (36)$$

which is solved as

$$v(t) = \frac{4V_0}{9\Sigma^2}\left(\frac{3}{4}\Sigma t + u_0\right)^3 + \int 6^{n/2}\frac{MQ}{\Sigma}\left(-\frac{2}{3}\ln\left(\frac{3}{4}\Sigma t + u_0\right)\right)^n dt \qquad (37)$$

Similar solutions are obtained by choosing $G(x) = Qe^x$, $G(x) = Qln(x)$ or $G(x) = Q\sqrt{x}$ in Eq. (23b). For $G(x) = Qe^x$, the corresponding point–like Lagrangian is given by

$$\mathcal{L} = 3a\dot{a}^2 - a^3\left(\frac{\dot{\phi}^2}{2} - V_0 e^{-\sqrt{3/2}\phi}\right) + MQe^{-\sqrt{6}\ln a + \phi}\,, \qquad (38)$$

and the transformed Lagrangian (38) becomes

$$\mathcal{L} = \frac{4}{3}\dot{u}\dot{v} + V_0 u^2 + MQu^{-\sqrt{8/3}}\,. \qquad (39)$$

Also in this case the variable v is cyclic and the quantity $\dfrac{\partial \mathcal{L}}{\partial \dot{v}} = \dfrac{4}{3}\dot{u}$ is conserved. The solution (31) is still valid and we can use it into the Jacobi first integral. The evolution equation for the variable v is

$$\dot{v} = \frac{V_0}{\Sigma}\left(\frac{3}{4}\Sigma t + u_0\right)^2 + \frac{MQ}{\Sigma}\left(\frac{3}{4}\Sigma t + u_0\right)^{-\sqrt{8/3}} \qquad (40)$$

7

and it admits the solution

$$v(t) = \frac{4V_0}{9\Sigma^2}\left(\frac{3}{4}\Sigma t + u_0\right)^3 + \frac{4MQ}{3\Sigma^2\left(-\sqrt{8/3}+1\right)}\left(\frac{3}{4}\Sigma t + u_0\right)^{-\sqrt{8/3}+1} + C \quad (41)$$

In the case $G(x) = Qln(x)$, the corresponding point–like Lagrangian is

$$\mathcal{L} = 3a\dot{a}^2 - a^3\left(\frac{\dot{\phi}^2}{2} - V_0 e^{-\sqrt{3/2}\phi}\right) + MQln(-\sqrt{6}\ln a + \phi), \quad (42)$$

and the transformed Lagrangian (42) assumes the form:

$$\mathcal{L} = \frac{4}{3}\dot{u}\dot{v} + V_0 u^2 + + MQln(-\sqrt{8/3}\ln u) \quad (43)$$

Since v is again a cyclic variable, the quantity $\dfrac{\partial\mathcal{L}}{\partial\dot{v}} = \dfrac{4}{3}\dot{u}$ is conserved and we get solution (31) again. Inserting (31) into the Jacobi first integral, we get the evolution equation for the variable v

$$\dot{v} = \frac{V_0}{\Sigma}\left(\frac{3}{4}\Sigma t + u_0\right)^2 + \frac{MQ}{\Sigma}ln\left(-\sqrt{8/3}\ln\left(\frac{3}{4}\Sigma t + u_0\right)\right) \quad (44)$$

which has solution

$$v(t) = \frac{4V_0}{9\Sigma^2}\left(\frac{3}{4}\Sigma t + u_0\right)^3 + \int\frac{MQ}{\Sigma}ln\left(-\sqrt{8/3}\ln\left(\frac{3}{4}\Sigma t + u_0\right)\right)dt \quad (45)$$

Finally, for $G(x) = Q\sqrt{x}$ the point–like Lagrangian is

$$\mathcal{L} = 3a\dot{a}^2 - a^3\left(\frac{\dot{\phi}^2}{2} - V_0 e^{-\sqrt{3/2}\phi}\right) + MQ\sqrt{(-\sqrt{6}\ln a + \phi)} \quad (46)$$

the transformed Lagrangian (46) can be written as

$$\mathcal{L} = \frac{4}{3}\dot{u}\dot{v} + V_0 u^2 + + MQ\sqrt{-\sqrt{8/3}\ln u}. \quad (47)$$

Due to the conservation of momentum $\dfrac{\partial\mathcal{L}}{\partial\dot{v}} = \dfrac{4}{3}\dot{u}$, the solution (31) holds again, while the Jacobi first integral yields the evolution equation for v

$$\dot{v} = \frac{V_0}{\Sigma}\left(\frac{3}{4}\Sigma t + u_0\right)^2 + \frac{MQ}{\Sigma}\sqrt{-\sqrt{8/3}\ln\left(\frac{3}{4}\Sigma t + u_0\right)} \quad (48)$$

8

The latter can be integrated as

$$v(t) = \frac{4V_0}{9\Sigma^2}\left(\frac{3}{4}\Sigma t + u_0\right)^3 + \int \frac{MQ}{\Sigma}\sqrt{-\sqrt{8/3}\ln\left(\frac{3}{4}\Sigma t + u_0\right)}\,dt =$$

$$\frac{4V_0}{9\Sigma^2}\left(\frac{3}{4}\Sigma t + u_0\right)^3 + \tag{49}$$

$$\frac{2^{3/4}\sqrt{-\log\left(\frac{3}{4}\left(\Sigma t + u_0\right)\right)}\left(-\frac{(\Sigma t + u_0)\mathcal{F}\left(\sqrt{\log\left(\frac{3}{4}(t\Sigma + u_0)\right)}\right)}{\sqrt{\log\left(\frac{3}{4}(\Sigma t + u_0)\right)}} + \Sigma t + u_0\right)}{\sqrt[4]{3}\Sigma}.$$

Here $\mathcal{F}$ is a Dawson integral, defined as:

$$\mathcal{F}(x) = e^{-x^2}\int_0^x e^{y^2}\,dy. \tag{50}$$

It is worth stressing that the Dawson integral can be represented in terms of the imaginary error function:

$$\mathcal{F}(x) = \frac{1}{2}\sqrt{\pi}e^{-x^2}\frac{erf(ix)}{i}. \tag{51}$$

3.2. The case of a phantom field

Almost all data sets from cosmological probes are compatible with dark energy equations of state parameter where $w < -1$ (see for instance [52]): dark energy with this kind of equations of state is often called phantom dark energy. Phantom fluids were first introduced by Caldwell, who suggested the name due to the circumstance that phantoms or ghosts possess negative energy, which leads to instabilities on both classical and quantum level [53–55], and violate the energy conditions. From the theoretical point of view, however, contexts with phantom-like equations of state, which do not lead to energy conditions violation, have been explored. Actually, phantom type of matter was investigated in several cosmological scenarios [56–60]. Here we consider phantom interacting dark energy, and look for general analytical form of the interaction and the self-interacting potential of the phantom field. The point–like Lagrangian is now of the form

$$\mathcal{L}(a, \phi, \dot{a}, \dot{\phi}) = 3a\dot{a}^2 + a^3\left(\frac{\dot{\phi}^2}{2} + V(\phi)\right) - 3ka + Ma^{-3(\gamma-1)}\left(1 + F(a, \phi)\right) \tag{52}$$

In this case, the conditions for the existence of a Noether symmetry (18) are

$$\alpha + 2a\frac{\partial\alpha}{\partial a} = 0, \tag{53a}$$

$$3\alpha + 2a\frac{\partial\beta}{\partial\phi} = 0 \tag{53b}$$

$$6\frac{\partial\alpha}{\partial\phi} + a^2\frac{\partial\beta}{\partial a} = 0, \tag{53c}$$

9

$$3\alpha a^2 V(\phi) + \beta a^3 \frac{dV}{d\phi}(\phi) - 3(\gamma - 1)Ma^{-3\gamma+2}\alpha\left(1 + F(a, \phi)\right) \quad (53d)$$

$$+ \quad Ma^{-3(\gamma-1)}\frac{\partial F}{\partial a}\alpha + Ma^{-3(\gamma-1)}\frac{\partial F}{\partial \phi}\beta - 3k\alpha = 0\,.$$

Once again by separating variables, Eqs. (53a), (53b) and (53c) have solutions of the form

$$\alpha = \frac{-A\cos\left(\frac{\sqrt{6}}{4}\phi\right) + B\sin\left(\frac{\sqrt{6}}{4}\phi\right)}{a^{1/2}}\,, \quad (54a)$$

$$\beta = \frac{A\sqrt{6}\sin\left(\frac{\sqrt{6}}{4}\phi\right) + B\sqrt{6}\cos\left(\frac{\sqrt{6}}{4}\phi\right)}{a^{3/2}}\,, \quad (54b)$$

where A and B are appropriate integration constants. By splitting again Eq. (53d) into

$$3\alpha a^2 V(\phi) + \beta a^3 V'(\phi) = 0\,, \quad (55a)$$

and

$$-3(\gamma-1)Ma^{-3\gamma+2}\alpha\left(1 + F(a, \phi)\right) + Ma^{-3(\gamma-1)}\frac{\partial F}{\partial a}\alpha + Ma^{-3(\gamma-1)}\frac{\partial F}{\partial \phi}\beta - 3k\alpha = 0\,, \quad (55b)$$

and, using Eqs. (54) , it turns out that

$$V(\phi) = V_0\left(B\cos\left(\frac{1}{2}\sqrt{\frac{3}{2}}\phi\right) - A\sin\left(\frac{1}{2}\sqrt{\frac{3}{2}}\phi\right)\right)^2\,. \quad (56)$$

Also in this case we can set $A = 0$ for simplicity, and we obtain solutions for $V(\phi)$ and $F(a, \phi)$ of the form

$$V(\phi) = V_0\cos^2\left(\frac{\sqrt{6}}{4}\phi\right)\,, \quad (57a)$$

$$F(a, \phi) = a^{3(\gamma-1)}G\left(\cos\left(\frac{\sqrt{6}}{4}\phi\right)a^{\frac{3}{2}}\right) + \frac{3k}{M}a^{3\gamma-2} - 1\,, \quad (57b)$$

where $G(x)$ denotes an arbitrary function of one real variable. Moreover, also in the case of a phantom scalar field, it turns out that the interaction term effectively cancels the contributions due to the spatial curvature and reduces the dynamic effect of the cosmological fluid to that of dust.

For instance, by choosing $G(x) = x$ and inserting expressions (57) into Eq. (52), the point–like Lagrangian assumes the form

$$\mathcal{L} = 3a\dot{a}^2 + a^3\left(\frac{\dot{\phi}^2}{2} + V_0\cos^2\left(\frac{\sqrt{6}}{4}\phi\right)\right) + M\cos\left(\frac{\sqrt{6}}{4}\phi\right)a^{\frac{3}{2}} \quad (58)$$

Therefore, also in the case of phantom scalar field, we can look for new coordinates u and v, solutions of Eqs.:

$$X(u) = 0 \quad \text{and} \quad X(v) = 1\,. \quad (59)$$

Again, under the hypothesis $A = 0$, they are given by

$$u(a, \phi) = f\left(\cos\left(\frac{\sqrt{6}}{4}\phi\right) a^{\frac{3}{2}}\right), \tag{60a}$$

$$v(a, \phi) = \frac{2}{3B}\sin\left(\frac{\sqrt{6}}{4}\phi\right) a^{\frac{3}{2}} + g\left(\cos\left(\frac{\sqrt{6}}{4}\phi\right) a^{\frac{3}{2}}\right), \tag{60b}$$

where f and g are arbitrary real functions of one variable. By setting $B = \frac{2}{3}$, $f(x) = x$ and $g(x) = 0$, we have

$$u(a, \phi) = \cos\left(\frac{\sqrt{6}}{4}\phi\right) a^{\frac{3}{2}}, \tag{61a}$$

$$v(a, \phi) = \sin\left(\frac{\sqrt{6}}{4}\phi\right) a^{\frac{3}{2}}. \tag{61b}$$

Inverting functions (61), we get the relations

$$a = \left(u^2 + v^2\right)^{\frac{1}{3}}, \tag{62a}$$

$$\phi = \frac{4}{\sqrt{6}}\arctan\left(\frac{v}{u}\right). \tag{62b}$$

Eqs. (62) allow us to express the Lagrangian (58) in the new coordinates as

$$\mathcal{L}(u, v, \dot{u}, \dot{v}) = \frac{4}{3}\left(\dot{u}^2 + \dot{v}^2\right) + V_0 u^2 + M u. \tag{63}$$

The Lagrange equations generated by the Lagrangian (63) are given by

$$\frac{8}{3}\ddot{u} - 2V_0 u - M = 0, \tag{64a}$$

$$\frac{8}{3}\ddot{v} = 0. \tag{64b}$$

Eqs. (64) admit solutions of the form

$$u(t) = C_1 e^{\frac{\sqrt{3V_0}t}{2}} + C_2 e^{-\frac{\sqrt{3V_0}t}{2}} - \frac{M}{2V_0}, \tag{65a}$$

$$v(t) = v_1 t + v_0. \tag{65b}$$

Similar solutions are obtained by choosing $G(x) = x^2$ in Eq. (57b). In this case, the point–like Lagrangian is expressed as

$$\mathcal{L} = 3a\dot{a}^2 + a^3\left(\frac{\dot{\phi}^2}{2} + V_0 \cos^2\left(\frac{\sqrt{6}}{4}\phi\right)\right) + M \cos^2\left(\frac{\sqrt{6}}{4}\phi\right) a^3. \tag{66}$$

11

Performing the change of coordinates (62), Lagrangian (66) assumes the form

$$\mathcal{L}(u, v, \dot{u}, \dot{v}) = \frac{4}{3}\left(\dot{u}^2 + \dot{v}^2\right) + (V_0 + M)\,u^2\,. \tag{67}$$

Lagrangian (67) yields the Euler– Lagrange equations

$$\frac{4}{3}\ddot{u} - (V_0 + M)\,u = 0\,, \tag{68a}$$

$$\frac{8}{3}\ddot{v} = 0\,. \tag{68b}$$

Eqs. (68) give solutions of the form

$$u(t) = C_1 e^{\frac{\sqrt{3(V_0+M)}t}{2}} + C_2 e^{-\frac{\sqrt{3(V_0+M)}t}{2}}\,, \tag{69a}$$

$$v(t) = v_1 t + v_0\,. \tag{69b}$$

In particular, for $V_0 = -M$, we have

$$u(t) = u_1 t + u_0\,. \tag{70}$$

More in general, we can chose $G(x) = x^n$ in Eq. (57b). The corresponding point–like Lagrangian is given by

$$\mathcal{L} = 3a\dot{a}^2 + a^3\left(\frac{\dot{\phi}^2}{2} + V_0 \cos^2\left(\frac{\sqrt{6}}{4}\phi\right)\right) + M\cos^n\left(\frac{\sqrt{6}}{4}\phi\right)a^{\frac{3n}{2}}\,. \tag{71}$$

In the new coordinates (62), Lagrangian (71) is expressed as

$$\mathcal{L}(u, v, \dot{u}, \dot{v}) = \frac{4}{3}\left(\dot{u}^2 + \dot{v}^2\right) + V_0 u^2 + M u^n\,. \tag{72}$$

The latter gives rise to Euler–Lagrange equations of the form

$$\frac{8}{3}\ddot{u} - 2V_0 u - nMu^{(n-1)} = 0\,, \tag{73a}$$

$$\frac{8}{3}\ddot{v} = 0\,. \tag{73b}$$

Eqs. (73) admit the following solutions

$$\pm\int \frac{2du}{\sqrt{3V_0 u^2 + 3nMu^n + C_1}} = t + C_2\,, \tag{74a}$$

$$v(t) = v_1 t + v_0\,. \tag{74b}$$

Similar solutions can be obtained by setting $G(x) = e^x$, $G(x) = ln(x)$ or $G(x) = \sqrt{x}$ in Eq. (57b). For $G(x) = e^x$, the corresponding point–like Lagrangian is given by

$$\mathcal{L} = 3a\dot{a}^2 + a^3\left(\frac{\dot{\phi}^2}{2} + V_0 \cos^2\left(\frac{\sqrt{6}}{4}\phi\right)\right) + Me^{cos\left(\frac{\sqrt{6}}{4}\phi\right)}a^{\frac{3}{2}}\,. \tag{75}$$

In the new coordinates (62), Lagrangian (75) is expressed as

$$\mathcal{L}(u, v, \dot{u}, \dot{v}) = \frac{4}{3} \left(\dot{u}^2 + \dot{v}^2 \right) + V_0 u^2 + M e^u \,. \tag{76}$$

From Eqs. (76), we derive Lagrange equations of the form

$$\frac{8}{3} \ddot{u} - 2 V_0 u - M e^u = 0 \,, \tag{77a}$$

$$\frac{8}{3} \ddot{v} = 0 \,. \tag{77b}$$

Eqs. (77) admit the following solutions

$$\pm \int \frac{2 du}{\sqrt{3 V_0 u^2 + 3 M e^u + C_1}} = t + C_2 \,, \tag{78a}$$

$$v(t) = v_1 t + v_0 \,. \tag{78b}$$

For $G(x) = ln(x)$, the point–like Lagrangian is

$$\mathcal{L} = 3 a \dot{a}^2 + a^3 \left(\frac{\dot{\phi}^2}{2} + V_0 \cos^2 \left(\frac{\sqrt{6}}{4} \phi \right) \right) + M ln \left(\cos \left(\frac{\sqrt{6}}{4} \phi \right) a^{\frac{3}{2}} \right) \,. \tag{79}$$

In the coordinates (62), Lagrangian (79) is expressed as

$$\mathcal{L}(u, v, \dot{u}, \dot{v}) = \frac{4}{3} \left(\dot{u}^2 + \dot{v}^2 \right) + V_0 u^2 + M ln(u) \,. \tag{80}$$

The induced Lagrange equations are of the form

$$\frac{8}{3} \ddot{u} - 2 V_0 u - \frac{M}{u} = 0 \,, \tag{81a}$$

$$\frac{8}{3} \ddot{v} = 0 \,. \tag{81b}$$

Solutions of (81) are

$$\pm \int \frac{2 du}{\sqrt{3 V_0 u^2 + 3 M ln(u) + C_1}} = t + C_2 \,, \tag{82a}$$

$$v(t) = v_1 t + v_0 \,. \tag{82b}$$

Finally, for $G(x) = \sqrt{x}$, the point–like Lagrangian is given by

$$\mathcal{L} = 3 a \dot{a}^2 + a^3 \left(\frac{\dot{\phi}^2}{2} + V_0 \cos^2 \left(\frac{\sqrt{6}}{4} \phi \right) \right) + M \sqrt{\left(\cos \left(\frac{\sqrt{6}}{4} \phi \right) a^{\frac{3}{2}} \right)} \,. \tag{83}$$

In the coordinates (62), Lagrangian (83) is expressed as

$$\mathcal{L}(u, v, \dot{u}, \dot{v}) = \frac{4}{3} \left(\dot{u}^2 + \dot{v}^2 \right) + V_0 u^2 + M \sqrt{u} \tag{84}$$

13

and the corresponding Euler–Lagrange equations are

$$\frac{8}{3}\ddot{u} - 2V_0 u - \frac{M}{2\sqrt{u}} = 0\,, \tag{85a}$$

$$\frac{8}{3}\ddot{v} = 0\,. \tag{85b}$$

Eqs. (85) admit the following solutions

$$\pm \int \frac{2du}{\sqrt{3V_0 u^2 + 3M\sqrt{u} + C_1}} = t + C_2\,, \tag{86a}$$

$$v(t) = v_1 t + v_0\,. \tag{86b}$$

As final remark, we observe that, in order to solve Eq. (53d) - or, analogously, Eq. (19d) -, it is possible to redefine $F(a, \phi)$ to absorb all terms, including the potential $V(\phi)$, into a single function:

$$F(a, \phi) \rightarrow \tilde{F}(a, \phi) = a^3 V(\phi) + Ma^{-3(\gamma-1)}(1 + F(a, \phi))\,. \tag{87}$$

It turns out that, using Eqs. (54) with $A = 0$,

$$F(a, \phi) = \frac{a^{3\gamma-3}\left(Mc_1\left[\sqrt{\frac{2}{3}}\left(2\log\left(\sec\left(\frac{1}{2}\sqrt{\frac{3}{2}}\phi\right)\right) - 3\log(a)\right)\right]\right)}{M}$$
$$-\frac{a^{3\gamma}V(\phi) - 3a^{3\gamma-2}k}{M} - 1\,, \tag{88}$$

where $c_1[x]$ is an arbitrary function of one real variable. For instance, by choosing

$$c_1\left[\sqrt{\frac{2}{3}}\left(2\log\left(\sec\left(\frac{1}{2}\sqrt{\frac{3}{2}}\phi\right)\right) - 3\log(a)\right)\right] = \tag{89}$$
$$\exp\left(-\frac{1}{3}m\left(2\log\left(\sec\left(\frac{1}{2}\sqrt{\frac{3}{2}}\phi\right)\right) - 3\log(a)\right)\right)\,,$$

we have the function $F(a, \phi)$ in the form:

$$F(a, \phi) = \frac{a^{3\gamma-3}\left(Ma^m\sec^{-\frac{2m}{3}}\left(\frac{1}{2}\sqrt{\frac{3}{2}}\phi\right) - a^3 V(\phi) - 3ak\right)}{M} - 1\,. \tag{90}$$

Inserting Eq. (90) into Eq. (52), Lagrangian (52) assumes the expression

$$\mathcal{L} = a^m \sec^{-\frac{2m}{3}}\left(\frac{1}{2}\sqrt{\frac{3}{2}}\phi\right) + \frac{a^3\dot{\phi}^2}{2} + 3a\dot{a}^2\,. \tag{91}$$

It turns out that this choice in Eq. (87) has no effect in the search for Noether symmetries and the results are the same with only a single function being involved. However, the form used in the action (52) offers the advantage to highlight contributions from different terms (scalar field potential, matter etc.).

14

4. Exact solutions as dark energy: comparison between theoretical prediction and observations

Let us show now that some of the above solutions can reproduce, both for the standard ($\epsilon = 1$) and the phantom scalar field ($\epsilon = -1$), the accelerated expansion of the Universe. In particular, they are compatible with different observational datasets, as the SNeIa Pantheon, the gamma ray bursts Hubble diagram, and measurements of the Hubble parameter.

4.1. The case of the standard scalar field

For our purposes, we consider the case described by the Eqs. (31) and (33) with $h = \dfrac{3}{2}$. It turns out that

$$u(t) = \frac{3\Sigma t}{4} + u_0 \tag{92}$$

$$v(t) = \frac{3}{8}t^2 \left(MQ + 2u_0 V_0\right) + \frac{tu_0 \left(MQ + u_0 V_0\right)}{\Sigma} + \frac{3}{16}\Sigma t^3 V_0\,.$$

The scale factor and the scalar field can be expressed as functions of $u(t)$ and $v(t)$. Actually $a(t) = (uv)^{1/3}$, and $\phi(t) = -\sqrt{2/3}\ln\frac{u}{v}$. Moreover we impose the condition $a(0) = 0$, and we set the age of the Universe, t_0, as time-scale ($t_0 = 1$). Therefore the expansion rate $H(t)$ is dimensionless, and its actual value $H_0 = H(t_0)$ is clearly of order 1. This means that it is numerically different from the Hubble constant usually measured in $\mathrm{kms^{-1}Mpc^{-1}}$. Actually, H_0 depends on the integration constants. We then set $a_0 = a(1) = 1$, and $H_0 = H(1)$. These conditions induce some constraints among the integration constants. By means of these choices the scale factor and the scalar field are parametrized by H_0, u_0 and Σ:

$$
\begin{aligned}
a^3(t) \;=\; & \frac{3\Sigma^2 t^4 \left(27\left(H_0 - 1\right)\Sigma^2 + 36\left(3H_0 - 2\right)\Sigma u_0 + 32\left(3H_0 - 1\right)u_0^2\right)}{\left(\Sigma + 4u_0\right)\left(3\Sigma + 4u_0\right)^3} + \\[1ex]
& \frac{4t^3 \left(\frac{27}{4}\left(4 - 3H_0\right)\Sigma^4 + 72\left(3H_0 - 2\right)\Sigma^2 u_0^2 + 80\left(3H_0 - 1\right)\Sigma u_0^3\right)}{\left(\Sigma + 4u_0\right)\left(3\Sigma + 4u_0\right)^3} + \\[1ex]
& \frac{4t^2 u_0 \left(27\left(4 - 3H_0\right)\Sigma^3 - 216\left(H_0 - 1\right)\Sigma^2 u_0 + 64\left(3H_0 - 1\right)u_0^3\right)}{\left(\Sigma + 4u_0\right)\left(3\Sigma + 4u_0\right)^3} + \\[1ex]
& \frac{32tu_0^2 \left(3\left(4 - 3H_0\right)\Sigma^2 - 30\left(H_0 - 1\right)\Sigma u_0 + 8\left(2 - 3H_0\right)u_0^2\right)}{\left(\Sigma + 4u_0\right)\left(3\Sigma + 4u_0\right)^3}\,,
\end{aligned}
\tag{93}
$$

$$e^{\sqrt{\frac{3}{2}}\phi} = \frac{v(t)}{u(t)} = \left(\frac{3\Sigma t}{4} + u_0\right)^{-1} \times \tag{94}$$

$$\left\{ \frac{4\Sigma t^3 \left(27\left(H_0 - 1\right)\Sigma^2 + 36\left(3H_0 - 2\right)\Sigma u_0 + 32\left(3H_0 - 1\right)u_0^2\right)}{\left(\Sigma + 4u_0\right)\left(3\Sigma + 4u_0\right)^3} + \right.$$

$$\frac{4t^2 \left(9\left(4 - 3H_0\right)\Sigma^3 - 36\left(H_0 - 1\right)\Sigma^2 u_0 + 48\left(3H_0 - 2\right)\Sigma u_0^2 + 64\left(3H_0 - 1\right)u_0^3\right)}{\left(\Sigma + 4u_0\right)\left(3\Sigma + 4u_0\right)^3}$$

$$\left. \frac{32tu_0 \left(3\left(4 - 3H_0\right)\Sigma^2 - 30\left(H_0 - 1\right)\Sigma u_0 + 8\left(2 - 3H_0\right)u_0^2\right)}{\left(\Sigma + 4u_0\right)\left(3\Sigma + 4u_0\right)^3} \right\} . \tag{95}$$

This exact solution provides an accelerated expansion as shown in Fig. 1.
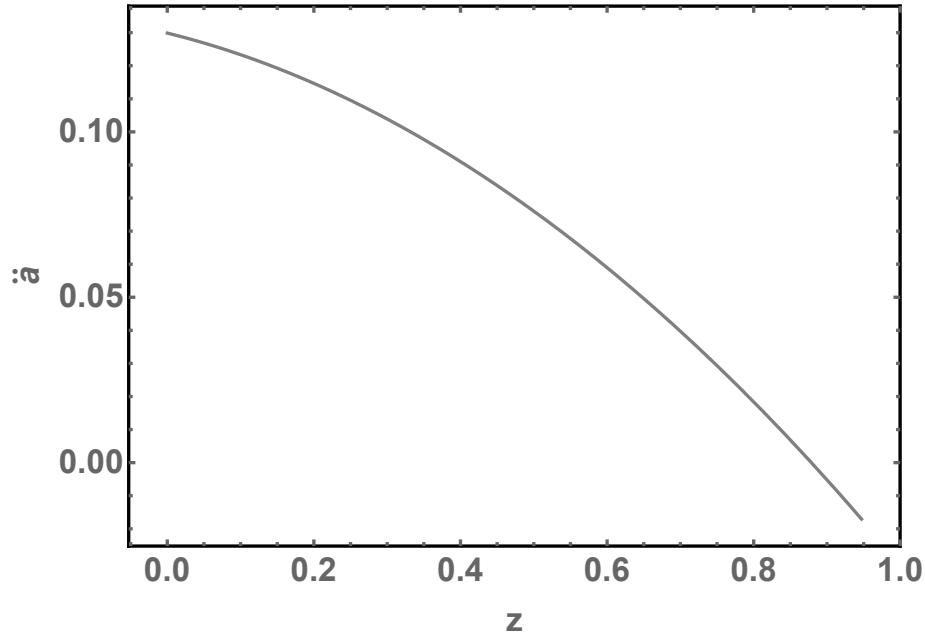
Figure 1: The redshift dependence of the acceleration for fixed value of $H_0 = 1$, $u_0 = 5.12$ and $\Sigma = 1.2$. The model provides an accelerated expansion and the transition to the decelerated regime occurs at a redshift compatible with observations.

Moreover, using the analytical expressions for $a(t)$ and $\phi(t)$, we can construct the standard quantities ρ_ϕ, p_ϕ, V_ϕ, w_ϕ, and the effective quantities ρ_ϕ^{eff}, p_ϕ^{eff}, and w_ϕ^{eff}, defined by Eqs. (11),(10),(12),(14) with $\epsilon = 1$. In Fig. 2, we compare the redshift behaviour of w_ϕ and w_ϕ^{eff} for some values of the parameters.

4.2. Supernovae and GRB Hubble diagram

The SNIa Hubble diagram provided the first strong evidence of the present accelerating expansion of the Universe. Here we consider the Pantheon compilation, con-
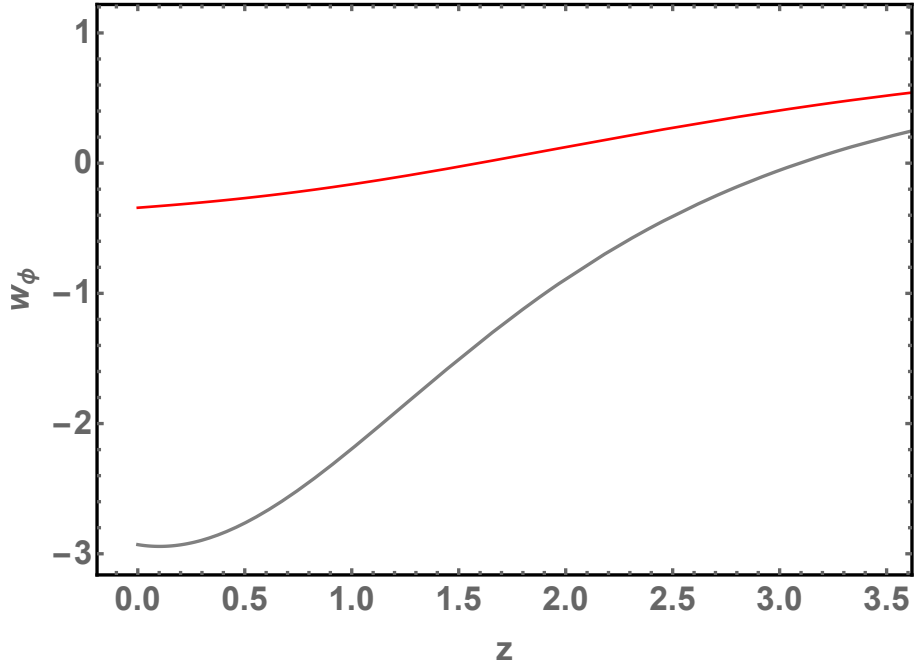
Figure 2: The redshift dependence of the equation of state parameter w_ϕ^{eff} (grey line) and w_ϕ (red line) for fixed value of $H_0 = 1$, $u_0 = 5.12$ and $\Sigma = 1.2$. The values of the parameters are chosen to highlight the different behavior between the two function: it is evident the *super-quintessential* nature of the equation of state ($w_\phi^{eff} < 1$) due to the interaction term.

sisting of 1048 SNIa in the range $0.01 < z < 2.26$. This sample combines 365 spectroscopically confirmed SNIa, discovered by the Pan-STARRS1 PS1 Medium Deep Survey, the subset of 279 PS1 SNIa in the range ($0.03 < z < 0.68$), distance estimates from SDSS, SNLS, and various low redshift and HST samples [4]. The SNIa observations provide the apparent magnitude $m(z)$, related to the Hubble free luminosity distance through the relation:

$$m_{th}(z) = \bar{M} + 5\log_{10}(D_L(z)).$$ (96)

Here $\bar{M}$ is the zero point offset and depends on the absolute magnitude M and on the Hubble parameter. The theoretical distance modulus is therefore defined as

$$\mu_{th}(z_i, \{\theta_p\}) = 5\log_{10}(D_L(z_i, \{\theta_p\})) + \nu_0,$$ (97)

where D_L is the luminosity distance:

$$D_L = \frac{c}{100h}(1+z)\int_0^z \frac{1}{H(\zeta, \theta)}d\zeta.$$ (98)

The parameter ν_0 in Eq. (97) encodes the Hubble constant. The absolute magnitude M and $\{\theta_p\}$ are the parameters of the model. Actually, it is well known that, using only

17

SNeIa, one cannot constrain the Hubble constant, without including measurements of its local value, since this is degenerate with M.

Gamma-ray bursts (GRBs) are the brightest cosmological sources in the Universe, thanks to the enormous amount of energy released in tens or hundreds of seconds: Actually the isotropic radiated energy, E_{iso}, can reach 10^{54} erg. Moreover their redshift distribution extends up to $z \sim 9.4$: therefore they are good candidates for cosmological investigation. Unfortunately GRBs are not standard candles, since their peak luminosity spans a wide range. However it is possible to consider them as distance indicators calibrating some empirical correlations of distance-dependent quantities and rest-frame observables. Here we consider the GRB Hubble diagram built up from the the $E_{\mathrm{p,i}}$-E_{iso} correlation. Actually, it is well known that GRBs have non-thermal spectra modeled by a smoothly broken power law with two indices (a low index α, and a high index β), named the band function,$N(E)$. Their spectra show a peak corresponding the photon energy $E_{\mathrm{p}} = E_0(2 + \alpha)$. Moreover, for GRBs with measured spectrum and redshift, it is possible to evaluate the intrinsic peak energy, $E_{\mathrm{p,i}} = E_{\mathrm{p}}(1 + z)$ and the isotropic equivalent radiated energy, defined as:

$$E_{\mathrm{iso}} = 4\pi D_L(z, \theta) \left(1 + z\right)^{-1} \int_{1/(1+z)}^{10^4/(1+z)} EN(E)\, dE\,, \qquad (99)$$

where

$$N(E) = \begin{cases} A \left(\frac{E}{100keV}\right)^\alpha \exp\left(-\frac{E}{E_0}\right) & (\alpha - \beta)\, E_0 \geq E \,, \\ A \left(\frac{(\alpha-\beta)E}{100keV}\right)^{\alpha-\beta} \exp\left(\alpha - \beta\right) \left(\frac{E}{100keV}\right)^\beta & (\alpha - \beta)\, E_0 \leq E \,. \end{cases}$$

The existence of a correlation between $E_{\mathrm{p,i}}$ and E_{iso} for long GRBs was discovered in 2002 [61], and was confirmed by later measurements by several different GRB detectors. It can be modeled as a linear relation between the logarithms of the two quantities:

$$\log\left[\frac{E_{\mathrm{p,i}}}{\mathrm{keV}}\right] = b + a \log\left[\frac{E_{\mathrm{iso}}}{10^{52}\ \mathrm{erg}}\right]\,, \qquad (100)$$

The $E_{\mathrm{p,i}}$–E_{iso} correlation is characterized by an intrinsic additional extra-Poissonian scatter, σ_{int}, around the best-fit line that has to be taken into account and determined together with (a, b) by the fitting procedure. After that values (a, b) are estimated, it is possible to obtain the energy E_{iso} of each burst at high redshift through Eq. 100, and the luminosity distance, $D_{\mathrm{L}}(z)$ from Eq. (99), building up the GRB Hubble diagram. Here we use the GRB Hubble diagram presented in [43], [62], and in [63]. In Fig. 3, we show the SNIa and GRB Hubble diagram.

4.3. Direct H(z) measurements

The accurate and direct determination of the expansion rate of the Universe, $H(z)$, has become one of the main drivers in precision cosmology, since it can provide fundamental information about the possible physical mechanisms underlying the late time acceleration. The Hubble parameter, defined as $H(z) = \dfrac{\dot{a}}{a}$, depends on the differential
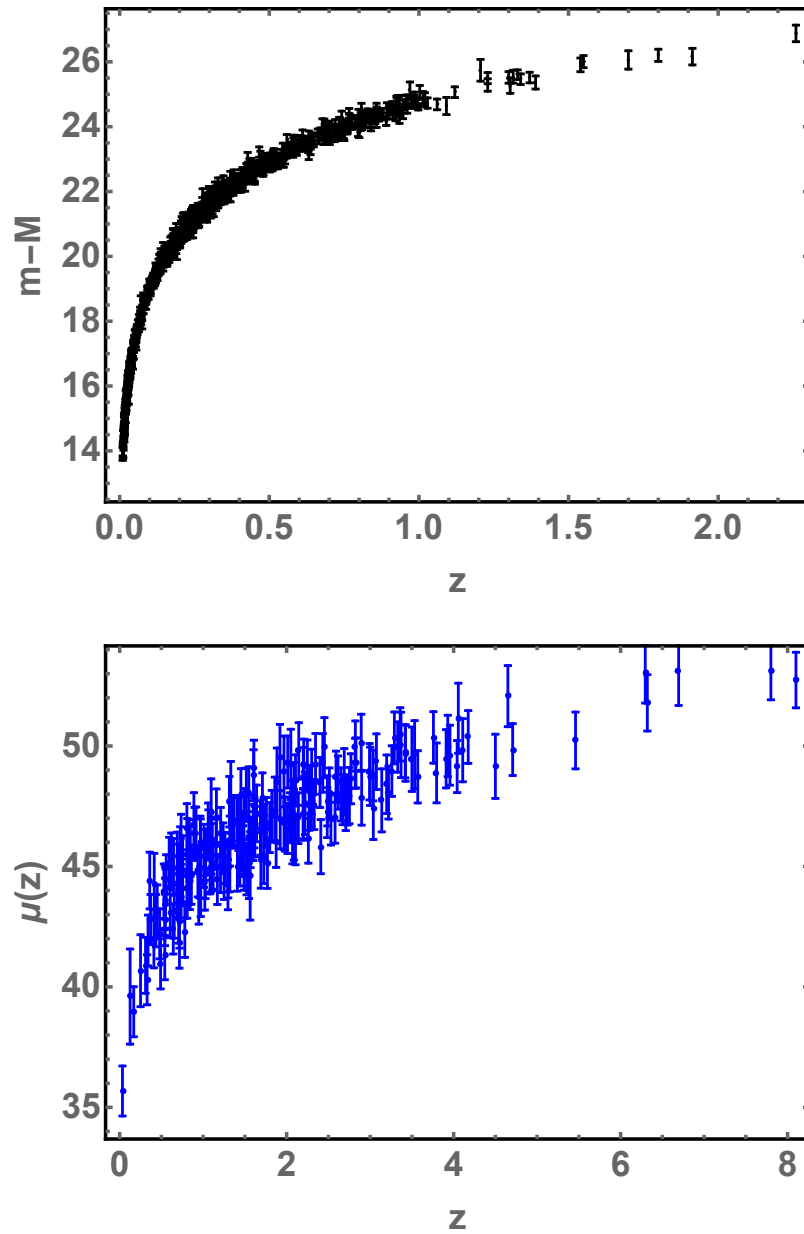
Figure 3: The Hubble diagram of SNIa (upper panel) and GRBs (lower panel), with their respective 1σ uncertainties.

age of the Universe as a function of redshift and can be measured using the cosmic chronometers. The quantity dz is obtained from spectroscopic surveys with high resolution, and the differential evolution of the age of the Universe dt in the redshift interval

dz can be measured provided that appropriate probes of the aging of the Universe, that is, just the cosmic chronometers, are identified. The most reliable cosmic chronometers, observable at high redshift, are old early-type galaxies evolving passively on a timescale much longer than their age difference. These galaxies formed the majority of their stars rapidly and early and they have not experienced subsequent major star formation or merging episodes. Moreover, the Hubble parameter can also be obtained from BAO measurements, observing the typical acoustic scale in the light-of-sight direction. Here we used a list of direct $H(z)$ measurements in the redshift range $z \sim 0.07 - 2.3$, compiled in [64], and [65], as shown in Fig.4
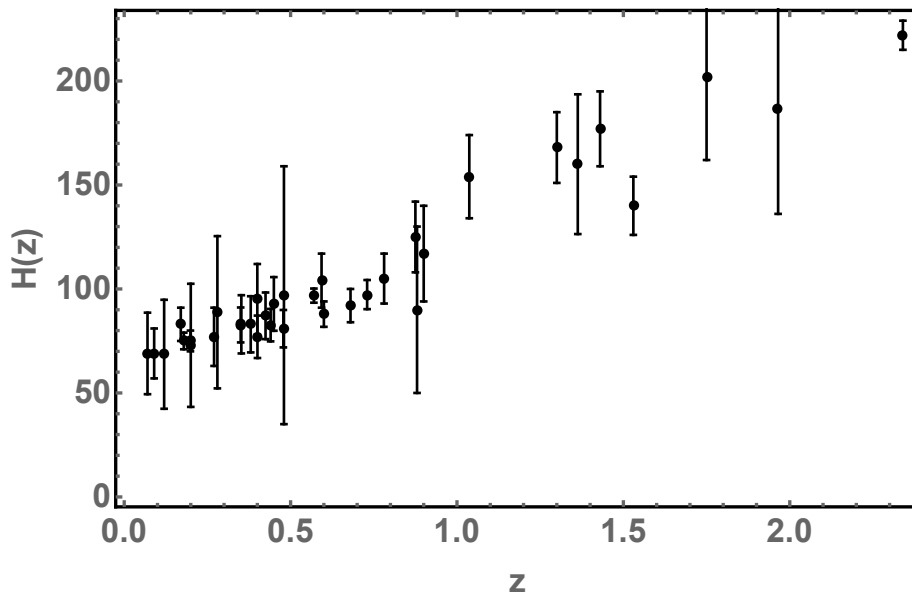

Figure 4: The direct $H(z)$ measurements used in our analysis.

4.4. Statistical analysis

To test the cosmological model described above, we use a Bayesian approach based on the Markov Chain Monte Carlo (MCMC) method [66]. We set the starting points for our chains performing a preliminary fit to maximize the likelihood function $\mathcal{L}(\mathbf{p})$:

$$
\begin{aligned}
\mathcal{L}(\mathbf{p}) \quad \propto \quad & \frac{\exp\left(-\chi^2_{SNIa/GRB}/2\right)}{(2\pi)^{\frac{\mathcal{N}_{SNIa/GRB}}{2}} |\mathbf{C}_{SNIa/GRB}|^{1/2}} \\
\times \quad & \frac{\exp\left(-\chi^2_H/2\right)}{(2\pi)^{\mathcal{N}_H/2} |\mathbf{C}_H|^{1/2}} ,
\end{aligned}
\tag{101}
$$

where

$$
\chi^2(\mathbf{p}) = \sum_{i,j=1}^{N} \left(x_i - x_i^{th}(\mathbf{p})\right) C_{ij}^{-1} \left(x_j - x_j^{th}(\mathbf{p})\right) .
\tag{102}
$$

20

Standard scalar field

Id	$\langle x \rangle$	$\tilde{x}$	68% CL	95% CL
SNIa /GRBs/H(z)				
H_0	1.01	1.02	(0.93, 1.08)	(0.90, 1.1)
u_0	5.17	4.2	(1.78, 8.3)	(1.07, 12.3)
Σ	1.5	1.1	(0.39, 2.9)	(0.14, 4.6)
h	0.7	0.69	(0.63, 0.77)	(0.61, 0.79)

Table 1: Constraints on the standard scalar field parameters from different data: combined SNIa and GRB Hubble diagrams, and $H(z)$ data sets. Columns show the mean $\langle x \rangle$ and median $\tilde{x}$ values and the 68% and 95% confidence limits.

In Eq.(102), $\mathbf{p}$ indicates the parameters of the cosmological model, N is the number of data points, x_i is the $i-th$ measurement, and $x_i^{th}(\mathbf{p})$ indicate the theoretical predictions. C_{ij} is the covariance matrix for the SNIa/GRB/H data. Moreover we used flat priors on the parameters , and we apply the Gelman–Rubin test for the convergence of the five running chains. We make thin the chains discarding the first 30% of iterations at the beginning of any run, and we finally extract the best fit values and the regions of confidence on the parameters by co-adding the thinned chains. In Table 1, we present the results of our analysis. In Figs. (5) and (6), we plot data vs theoretical predictions.

4.5. The case of the phantom scalar field

Also the phantom scalar field, selected by the Noether symmetry, can provide a late accelerated expansion. Let us consider the case described by the Eqs. (69a) and (69b). It is $a(t) = \left(u(t)^2 + v(t)^2\right)^{1/3}$, and $\phi(t) = \dfrac{4}{\sqrt{6}}\arctan\left(\dfrac{v(t)}{u(t)}\right)$.

Also in this case we impose the condition $a(0) = 0$, and we set the the age of the Universe, t_0, as a time-scale ($t_0 = 1$). Indeed, we set $a_0 = a(1) = 1$, and $H_0 = H(1)$. These conditions induce constraints among the integration constants: The scale factor and the scalar field are therefore parametrized by H_0, and α (where $\alpha = \sqrt{3\left(V_0 + M\right)}$).

By the analytical expressions for $a(t)$ and $\phi(t)$, we can construct the standard quantities $\rho_\phi, p_\phi, V_\phi, w_\phi$, and the effective quantities $\rho_\phi^{eff}, p_\phi^{eff}$, and w_ϕ^{eff}, defined by Eqs. (11),(10),(12),(14) with $\epsilon = -1$. It is worth noticing that in order to evaluate the interaction contribution to the effective quantities, we parametrize the present matter
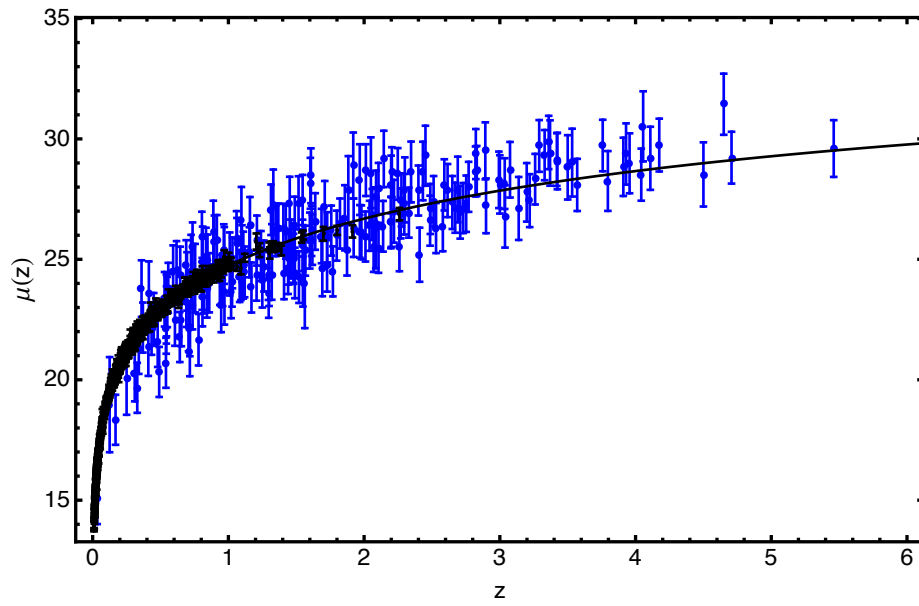
Figure 5: Comparison between GRB and Pantheon data vs theoretical distance modulus, corresponding to the best fit values of the parameters.
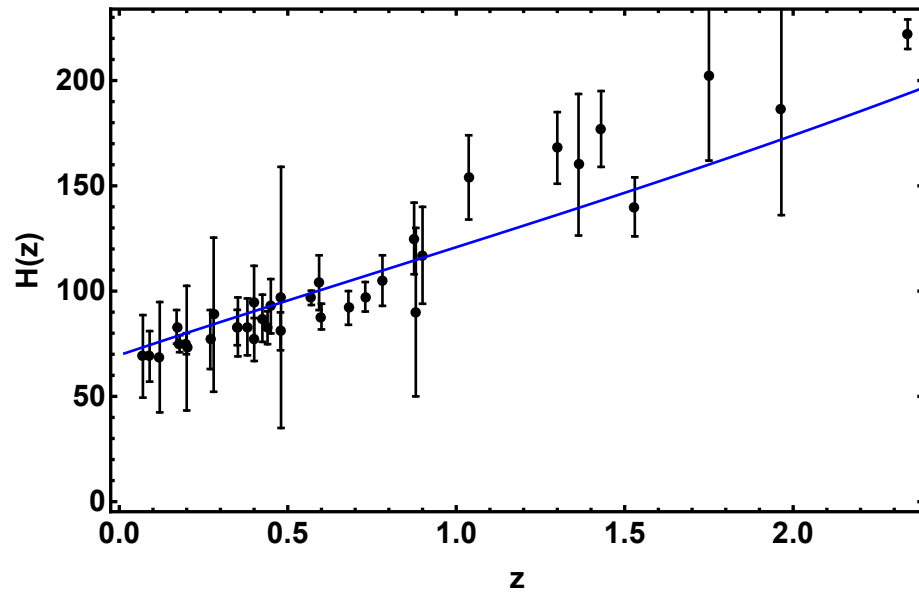

Figure 6: Comparison between the $H(z)$ data vs the theoretical predictions, corresponding to the best fit values of the parameters.

density, M, in terms of the associated $\Omega_M = \dfrac{M}{3H_0^2}$. In Fig. 7, we compare the red-shift behaviour of w_ϕ and w_ϕ^{eff} for some values of the parameters. In order to test this model, we use the same data-samples, and we apply the same statistical analysis described above. In Table 2, we present the results of our analysis.
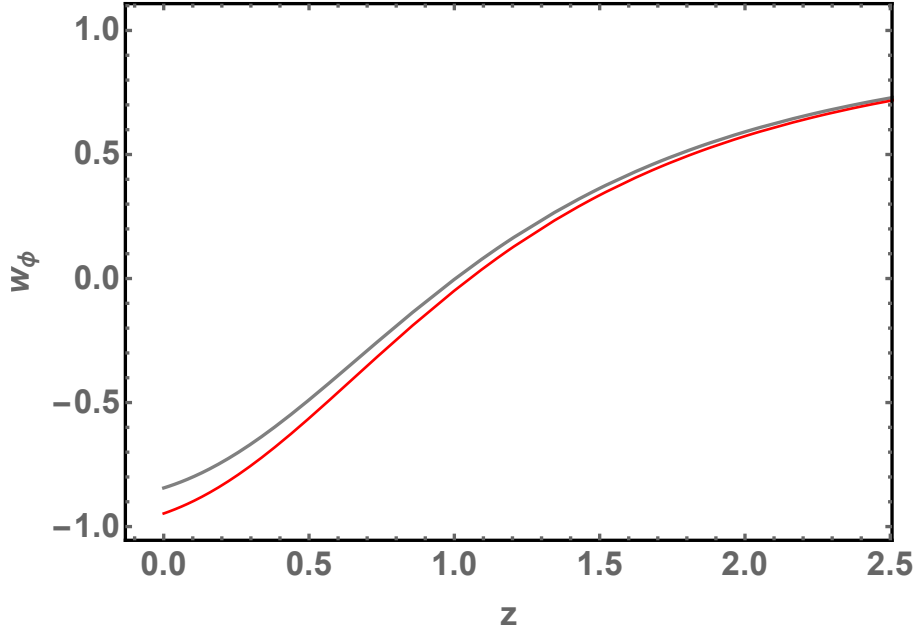

Figure 7: The redshift dependence of the equation of state parameter w_ϕ^{eff} (red line) and w_ϕ (gray line) for fixed value of $H_0 = 0.98$, $\alpha = 3.2$ and $\Omega_m = 0.27$.

5. Discussion and Conclusions

We analyzed non-flat cosmological models with an interacting quintessence component, where, in turn, a standard or a phantom scalar field interacts with the dark matter term. These models are usually characterized by a phenomenological choice of the form of the interaction. Instead, we used the Noether symmetry approach to select the analytical form of both the scalar-field self-interaction potential and the interaction term. It turns out that this latter cancels out the contributions due to the spatial curvature and reduces the dynamic effect of cosmological fluid to that of dust. Of course, there are still effects of curvature in the evolution of the scalar field, as it can be inferred from the definition of the scalar field effective density and pressure.

Furthermore, we were able to obtain exact solutions of the cosmological equations, some of which can reproduce the accelerated expansion of the Universe, both in the case of a standard and a phantom scalar field. Moreover, some solutions make evident the so called super-quintessential behaviour of the equation of state (i.e: $w_\phi^{eff} < -1$)

Phantom scalar field

Id	$\langle x \rangle$	$\tilde{x}$	68% CL	95% CL
SNIa /GRBs/H(z)				
H_0	0.95	0.96	(0.93, 1.2)	(0.90, 1.3)
α	7.8	7.9	(5.8, 9.3)	(4.2, 10.3)
h	0.72	0.72	(0.65, 0.78)	(0.63, 0.80)

Table 2: Constraints on the phantom scalar field parameters from different data samples (combined SNIa and GRB Hubble diagrams, and $H(z)$ data sets. Columns show the mean $\langle x \rangle$ and median $\tilde{x}$ values and the 68% and 95% confidence limits.

due to the coupling term. Finally, we showed that some of the exact solutions are compatible with different observational dataset related to the background expansion, as the SNeIa Pantheon data, a GRBs Hubble diagram, and direct measurements of the Hubble parameter. In a forthcoming paper, we are going to perform a detailed analysis of the interacting dark energy on the large scale structures. This approach can allow us to achieve a reliable cosmic history at different redshifts.

Acknowledgements

References

[1] A.G. Riess, L.G. Strolger, S. Casertano, H.C. Ferguson, B. Mobasher, et al., 2007, ApJ, 659, 98

[2] Suzuki et al. (The Supernova Cosmology Project), ApJ, **46**, (2012) 85

[3] Planck Collaboration, 2016, Astronomy & Astrophysics, **594**, A13

[4] D. M. Scolnic, D.O. Jones, A. Rest, et al. 2018, ApJ, **859**, 101

[5] S. M. Perlmutter, G. Aldering, M. Della Valle, S. Deustua, R.S. Ellis, R. S., et al, Nature, **391**, (1998) 51

[6] S. M. Perlmutter, G. Aldering, . G. Goldhaber, R. Knop, P. Nugent, et al., ApJ, **517**, (1999) 565

[7] R. Arona, W Cardona, S. Nesseris, Phys. Rev. D **99** (2019) 043516

[8] Y-F. Cai, S. Capozziello, M. De Laurentis, E. N. Saridakis Rept. Prog. Phys. **79** (2016) 106901.

[9] M. Demianski, E. Piedipalumbo, C. Rubano, C. Tortora, 2006, Astron.Astrophys., **454**, 55-66

[10] S. Nesseris, D. Sapone, S. Sypas, Phys.Dark Univ. **27**, (2020) 100413

[11] S. Nojiri and S. D. Odintsov, Phys. Rept. **505** (2011) 59

[12] S. Capozziello and M. De Laurentis, Phys. Rept. **509** (2011) 167

[13] S. Nojiri, S. D. Odintsov and V. K. Oikonomou, Phys. Rept. **692** (2017) 1

[14] M. Demianski, E. Piedipalumbo, C. Rubano, P. Scudellaro, 2008, Astron. & Astrophys., **481**, 279

[15] E. Piedipalumbo, E. Della Moglie, R. Cianci, 2015, IJMPD, **24**, 1550100. doi:10.1142/S021827181550100X

[16] S. Bahamonde, C. Boehmer, G. Christian, S. Carloni, E.J. Copeland, W .Fang, N. Tamanini, 2018, Physics Reports, **775**, 1-122

[17] T. Damour, G.W. Gibbons and C. Gundlach, Phys. Rev. Lett. **64**, 123 (1990); J.A. Casas, J. Garcia-Bellido and M. Quiros, 1992, Clas. Quant. Grav. **9**, 1371; R. Bean, 2001, Phys. Rev. D **64**, 123516; D. Comelli, M. Pietroni and A. Riotto, 2003, Phys. Lett. B **571**, 115; U. Franca and R. Rosenfeld, 2004,Phys. Rev. D **69**, 063517 (2004); L. P. Chimento, A. S. Jakubi, D. Pavon and W. Zimdahl, 2003, Phys. Rev. D **67**, 083513

[18] L. Amendola, Phys. Rev. D **62**, 043511 (2000); L. Amendola and D. Tocchini-Valentini, Phys. Rev. D **64**, 043509 (2001); L. Amendola, C. Quercellini, D. Tocchini-Valentini and A. Pasqui, Astrophys. J. **583**, L53 (2003); L. Amendola and C. Quercellini, Phys. Rev. D **68**, 023514 (2003); G. Olivares, F. Atrio-Barandela and D. Pavon, Phys. Rev. D **71**, 063523 (2005); Amendola, L., Appleby, S., Avgoustidis, A. et al. Living Rev Relativity (2018) 21: 2.

[19] J. Khoury and A. Weltman, 2004, Phys. Rev. Lett. **93**, 172204; J. Khoury and A. Weltman, 2004, Phys. Rev. D **69**, 044026; S.S. Gubser and J. Khoury, 2004, Phys. Rev. D **70**, 104001.

[20] P. Brax, C. van de Bruck, A.C. Davis, J. Khoury and A. Weltman, Phys. Rev. D **70**, 123518 (2004)

[21] H. Wei and R. G. Cai, 2005, Phys. Rev. D **71**, 043504

[22] G.R. Farrar and P.J.E. Peebles, 2004, Astrophys. J. **604**, 1; S.S. Gubser and P.J.E. Peebles, 2004, Phys. Rev. D**70**, 123510

[23] D.B. Kaplan, A.E. Nelson and N. Weiner, 2004, Phys. Rev. Lett. **93**, 091801; R. D. Peccei, 2005, Phys. Rev. D**71**, 023527

[24] S. Das, P. Corasaniti and J. Khoury, 2006, Phys. Rev.D **73**, 083509

[25] D.. Boriero, S. Das, Yvonne Y. Y. Wong, 2015, JCAP, **07**,33

[26] S.A. Bonometto, M. Mezzetti, R. Mainini, 2017, JCAP, **10**, 011

[27] S.A.Bonometto, R. Mainini, M. Mezzetti, 2019, MNRAS, **486**,2321

[28] M. Demianski, C. Rubano, C. Tortora, 2005, Astron.Astrophys. **431**, 27-43

[29] A.K. Sanyal, IJMP A, 2007, **22**, 1301

[30] S. Capozziello, R. D'Agostino, O. Luongo, I.J.Mod.Phys. D **28**, 1930016 (2019).

[31] Piedipalumbo E., De Laurentis M., Capozziello S., 2020, PDU, 27, 100444. doi:10.1016/j.dark.2019.100444

[32] F. Bajardi and S. Capozziello, *Noether Symmetries in Theories of Gravity*," Cambridge University Press, Cambridge (2022). doi:10.1017/9781009208727

[33] R. de Ritis, G. Marmo, G. Platania, C. Rubano, P. Scudellaro, and C. Stornaiolo, 1990, Phys. Rev. D **42**, 1091

[34] S. Capozziello, R. de Ritis, C. Rubano, and P. Scudellaro, 1996 , Riv. Nuovo Cim. **19 (4)**,1

[35] S. Capozziello and A. De Felice, JCAP **0808** (2008) 016.

[36] S. Capozziello, M. De Laurentis and S. D. Odintsov, Mod. Phys. Lett. A **29** (2014) no.30, 1450164

[37] S. Basilakos, S. Capozziello, M. De Laurentis, A. Paliathanasis and M. Tsamparlis, Phys. Rev. D **88** (2013) 103526

[38] S. Capozziello, E. Piedipalumbo, C. Rubano, P. Scudellaro, Astronomy & Astrophysics, **505**, 21 (2008).

[39] A. K. Sanyal, C. Rubano, and E. Piedipalumbo, Gen. Rel. and Grav., **35**, (2003) 1617

[40] A. K. Sanyal, B. Modak, C. Rubano, and E. Piedipalumbo, Gen. Rel. and Grav., **37**, (2005) 407

[41] F. Lucchin and S. Matarrese, Phys. Rev. D **32** (1985), 1316

[42] S. Capozziello, Int. J. Mod. Phys. D **11** (2002), 483.

[43] M. Demianski, E. Piedipalumbo, D. Sawant, L. Amati, Astronomy & Astrophysics, **598**, (2017b) A113

[44] V. Faraoni, *Cosmology in Scalar-tensor Gravity*, Fundamental Theories of Physics, Ed. Springer, Dordrecht (2011).

[45] J. M. Overduin and P. S. Wesson. Kaluza-Klein Gravity. Phys. Rept. **283**, 303 (1997).

[46] N.D.Birrell, and P.C.W.Davies, *Quantum fields in curved space*, *Cambridge University Press*, **7**, (1984).

[47] B. Saha, 2015, *Astrophys. Space Sci.* **357**, 28.

[48] A.Joyce, L.Lombriser,F.Schmidt, 2016, Annual Review of Nuclear and Particle Science,**66**, 95-122

[49] M. Demianski & E. Piedipalumbo, Eur.Phys.J. C, **79** (2019), 575

[50] S. Vignolo, S. Carloni and L. Fabbri, 2015, Phys. Rev. D **91**, 043528.

[51] S. Carloni, R. Cianci, P. Feola, E. Piedipalumbo, S. Vignolo, JCAP **09** (2019), 014.

[52] Planck Collaboration, N. Aghanim, Y. Akrami, M. Ashdown, J. Aumont, C. Baccigalupi, M. Ballardini, et al., Astronomy & Astrophysics, **641**, A6 (2020) doi:10.1051/0004-6361/201833910

[53] R. R. Caldwell, Phys. Lett. B **545**, 23 (2002).

[54] S. M. Carroll, M. Hofman, and M. Trodden, Phys. Rev. D **68**, 023509 (2003); S. D. H. Hsu, A. Jenkins, and M. B. Wise, Phys. Lett. B **597**, 270 (2004)

[55] S. Nojiri and S. D. Odintsov, Phys. Lett. B **595**, 1 (2004); Phys. Rev. D **70**, 103522 (2004).

[56] K. J. Ludwick, MPLA, **32**, 1730025 (2017) doi:10.1142/S0217732317300257

[57] S. Nojiri, S. D. Odintsov, M.Sami, PhRvD, **74** (2006), 046004. doi:10.1103/PhysRevD.74.046004

[58] J.A., Vázquez, D. Tamayo, A.A. Sen, and I. Quiros, 2021, Physical Review D **103** (2021), 043506. doi:10.1103/PhysRevD.103.043506.

[59] F. Bargach, A. Bargach, M. Bouhmadi-López, A. Errahmani, and T. Ouali, International Journal of Modern Physics D **30** (2021), 2150076-9. doi:10.1142/S0218271821500760.

[60] Y. Kucukakca, IJGMM, **17** (2020), 2050179-1038. doi:10.1142/S0219887820501790

[61] Amati, L., Frontera, F., Tavani, M., in't Zand, J.J.J, Antonelli, A., Costa, E., Feroci, M., Guidorzi, C., Heise, J., Masetti, N., Montanari, E., Nicastro, L., Palazzi, E., et al., A&A, **390** (2002) 81

[62] M. Demianski, E. Piedipalumbo, D. Sawant, L. Amati, MNRAS, **506**, 903 (2021) doi:10.1093/mnras/stab1669

[63] M. Moresco, L. Amati, L. Amendola, S. Birrer, J. P. Blakeslee, M. Cantiello, A. Cimatti, et al., LRR, **25**, 6 (2022) doi:10.1007/s41114-022-00040-z

[64] M.. Moresco, L.. Pozzetti, A.. Cimatti, R.. Jimenez, C.. Maraston, L.. Verde, D. Thomas, et al., JCAP, 2016, **014**. doi:10.1088/1475-7516/2016/05/014

[65] R.-Y. Guo, X. Zhang, EPJC, **76**, 163 (2016). doi:10.1140/epjc/s10052-016-4016-x

[66] J. Dunkley, M. Bucher, P. G. Ferreira, K. Moodley and C. Skordis, Mon. Not. Roy. Astron. Soc. **356** (2005), 925. doi:10.1111/j.1365-2966.2004.08464.x